Speed control of electrical submersible pumps using fuzzy logic control

Saleh M. El-koliel[1], Hussein Eleissawi[2], Adel S. Nada[1]
[1]Faculty of Engineering, Electrical Engineering Department, Al-Azhar University, Cairo, Egypt
[2]Reactors Department, Egyptian Atomic Energy Authority, Cairo, Egypt

Article Info	ABSTRACT
	Electrical submersible pumps (ESPs) are multistage centrifugal pumps driven by specially designed three-phase induction motors. They are used in many applications such as nuclear and petroleum industries. In the presented paper, we study the speed control of an ESP pump using a rule-based fuzzy logic controller (FLC). As a case study, an oil well is considered to analyze the effects of changing the speed of an ESP pump on both the ESP pump and motor parameters. The proposed speed control model of ESP pumps provides the ability to optimize wells production and power consumption, as well as soft starting of ESP motors. This is done by using a variable speed drive (VSD), which changes the frequency of the voltage supplied to the ESP motor. The utilized VSD model consists of a two-level voltage source inverter (VSI), space vector pulse width modulator (SVPWM) and a rule-based fuzzy logic speed controller. Also, in this study a dynamic hydraulic model of an oil well is implemented. In this study, a mathematical model of the ESP motor and ESP pump is developed. The obtained simulation results show that the combination of the FLC speed Controller and SVPWM provides a faster and more effective method of controlling the speed of electrical submersible pumps than the conventional PID speed controllers. The MATLAB/Simulink software is used to achieve simulative validation of the complete system.

Corresponding Author:

Saleh M. El-koliel
Electrical Engineering Department, Al-Azhar University
Cairo, Egypt
Email: saleh.el.koliel@gmail.com

1. INTRODUCTION

Electrical submersible pumps (ESPs) are widely used in many applications. For example, in the nuclear field, submersible pumps are used in the low-pressure injection system (LPIS) of nuclear power plants [1]. LPIS is a safety system, which interferes to reduce the impact of a loss of coolant accidents (LOCAs). Also, it may be used in groundwater monitoring wells which provide samples for detecting releases and contaminations which may result from the operation of the nuclear reactors. In the petroleum industry, electrical submersible pumps (ESP) are multi-stage centrifugal pumps driven by three-phase induction motors. They are used to lift fluids from oil wells to the surface when bottom-hole pressures are not sufficient, or when higher production rates are needed [2]. The speed control of ESP pumps is crucial for soft starting their electric motors [3], [4], optimizing production rates [5], as well as, saving energy [6], [7]. In addition, matching the required power of the ESP pump with the available power supply to ensure secure electrical feedings, i.e., optimizing the energy utilization [8], [9], especially at remote oilfield locations. In order to study the effects of speed change of ESP pumps, a combined fluid mechanics, electrical and

mechanical models of an ESP oil well system are needed. A dynamic model of an ESP deep geothermal well was developed by Kulick *et al.* [10], but the speed controller was not taken into consideration. Another model was presented for controller development [11], but neither ESP electric motor nor variable speed drive were included. Many works were found in the literature, which aimed to provide more effective methods of controlling the speed of induction motors, but three are no published papers have replaced the conventional control methods such as PID with more effective control methods such as FLC to control the speed of a complete electrical submersible pump system i.e., variable speed drive variable speed drive (VSD), ESP pump, ESP motor, and hydraulic oil well models.

The main objective of this paper is to develop a complete ESP oil well model as presented in Figure 1. The proposed model consists of a mathematical dynamic model of an oil well taking into consideration the pressure loss due to friction in pipes and the inflow performance of the reservoir. In addition, ESP pump and electric motor mathematical models were implemented in the system. Also, a variable speed drive with a space vector pulse width modulation (SVPWM) switching algorithm and rule-based fuzzy logic (FLC) speed controller has been utilized. The presented model helps to better understand the effect of changing the speed of ESP pumps on the different parameters of the system. Also, it could be used as an algorithm to automatically control the operation of ESP oil wells.
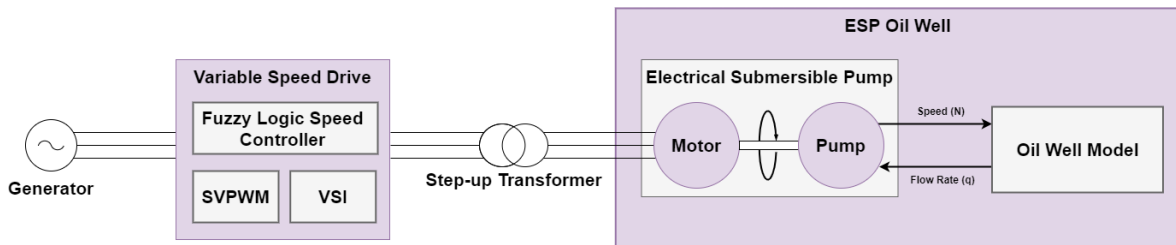

Figure 1. The complete model of an ESP oil well

2.   RESEARCH METHOD

To understand the effect of changing the speed of ESP oil wells on the parameters of the entire system, first, models for each element of the system are created i.e., VSD, ESP pump, ESP motor, and hydraulic oil well models. Then a simulation for the complete system was run based on a real-world scenario using PID and FLC controllers in order to get the results and perform a performance comparison between the two approaches.

2.1. ESP motor model

ESP motor is basically a three-phase induction motor [12], [13]. The Mathematical motor model was developed by using the reference frame theory [14], [15]. A three-phase induction motor can be converted to a two-phase in the dq0 reference frame by using park transformation as in Figure 2.
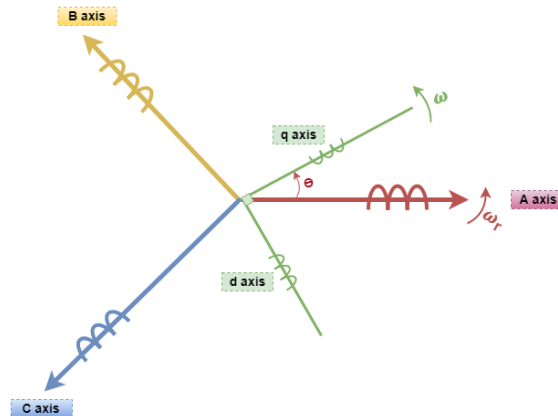

Figure 2. Park (ABC to dq0) transformation

The purpose of this transformation is to simplify the calculations and to make the flux linkage of each winding independent of the current in the other windings [16]. The transformation of stator and rotor parameters from the (abc) system to the (dq0) system can be done as in (1) and (2), respectively.

$$f_{qd0s} = K_s\, f_{abcs} \tag{1}$$

$$f_{qd0r} = K_r\, f_{abcr} \tag{2}$$

Where,

$$K_s = \frac{2}{3} \begin{bmatrix} \cos(\theta) & \cos(\theta - \frac{2\pi}{3}) & \cos(\theta - \frac{4\pi}{3}) \\ \sin(\theta) & \sin(\theta - \frac{2\pi}{3}) & \sin(\theta - \frac{4\pi}{3}) \\ \frac{1}{2} & \frac{1}{2} & \frac{1}{2} \end{bmatrix} \tag{3}$$

$$K_r = \frac{2}{3} \begin{bmatrix} \cos(\beta) & \cos(\beta - \frac{2\pi}{3}) & \cos(\beta + \frac{4\pi}{3}) \\ \sin(\beta) & \sin(\beta - \frac{2\pi}{3}) & \sin(\beta + \frac{4\pi}{3}) \\ \frac{1}{2} & \frac{1}{2} & \frac{1}{2} \end{bmatrix} \tag{4}$$

Where, f can be any variable such as current, voltage, or flux linkage. θ and θr are the angles between a-axis and q-axis of the stator and between a-axis of the stator and a-axis of the rotor, respectively, while, $\beta = \theta - \theta r$. The stator and rotor voltages can be obtained in the dq0 frame [16], as in from (5) to (10).

$$v_{qs} = r_s i_{qs} + \frac{\omega}{\omega_b}\psi_{ds} + \frac{1}{\omega_b}\frac{d\psi_{qs}}{dt} \tag{5}$$

$$v_{ds} = r_s i_{ds} - \frac{\omega}{\omega_b}\psi_{qs} + \frac{1}{\omega_b}\frac{d\psi_{ds}}{dt} \tag{6}$$

$$v_{0s} = r_s i_{0s} + \frac{1}{\omega_b}\frac{d\psi_{0s}}{dt} \tag{7}$$

$$v'_{qr} = r'_r i'_{qr} + \frac{\omega - \omega_r}{\omega_b}\psi'_{dr} + \frac{1}{\omega_b}\frac{d\psi'_{qr}}{dt} \tag{8}$$

$$v'_{dr} = r'_r i'_{dr} + \frac{\omega - \omega_r}{\omega_b}\psi'_{qr} + \frac{1}{\omega_b}\frac{d\psi'_{dr}}{dt} \tag{9}$$

$$v'_{0r} = r'_r i'_{0r} + \frac{1}{\omega_b}\frac{d\psi'_{0r}}{dt} \tag{10}$$

Where, ω, ω_r, ω_b, r_s, and r'_r are the reference frame speed, rotor speed, base speed, stator winding resistance, and rotor winding resistance, respectively. Also, ψ_{qs}, ψ_{ds}, ψ'_{qr}, and ψ'_{dr} are the stator q-axis flux linkage, stator d-axis flux linkage, rotor q-axis flux linkage, and rotor d-axis flux linkage, respectively. i_{qs}, i_{ds}, i'_{qr} and i'_{dr} are the stator q-axis current, the stator d-axis current, the rotor q-axis current, and the rotor d-axis current, respectively. The stator and rotor flux linkage equations in the dq0 frame can be represented as in from (11) to (16).

$$\psi_{qs} = X_{ls} i_{qs} + \psi_{mq} \tag{11}$$

$$\psi_{ds} = X_{ls} i_{ds} + \psi_{md} \tag{12}$$

$$\psi_{0s} = X_{ls} i_{0s} \tag{13}$$

$$\psi'_{qr} = X'_{lr} i'_{qr} + \psi_{mq} \tag{14}$$

$$\psi'_{dr} = X'_{lr} i'_{dr} + \psi_{md} \tag{15}$$

$$\psi'_{0r} = X'_{lr} i'_{0r} \tag{16}$$

Where,

$$\psi_{mq} = X_{aq} \left(\frac{\psi_{qs}}{X_{ls}} + \frac{\psi'_{qr}}{X'_{lr}} \right) \tag{17}$$

$$\psi_{md} = X_{ad} \left(\frac{\psi_{ds}}{X_{ls}} + \frac{\psi'_{dr}}{X'_{lr}} \right) \tag{18}$$

$$X_{aq} = X_{ad} = \left(\frac{1}{X_m} + \frac{1}{X_{ls}} + \frac{1}{X'_{lr}} \right)^{-1} \tag{19}$$

The electromagnetic torque T_e of induction motors is given by (20):

$$T_e = \frac{3}{2} \frac{p}{2\omega_b} (\psi_{ds} i_{qs} - \psi_{qs} i_{ds}) \tag{20}$$

Where, p is the number of poles. Electromagnetic torque T_e is related to rotor mechanical speed ω_{rm} by (21):

$$T_e = J \frac{d\omega_{rm}}{dt} + F\omega_{rm} + T_l \tag{21}$$

Where, J, F, and T_l are the rotor inertia, friction factor, and load torque, respectively. Equations from (5) to (21) are used to build the ESP motor in the stationary reference frame (i.e., $\omega = 0$) in MATLAB/SIMULINK® software as shown in Figure 3.
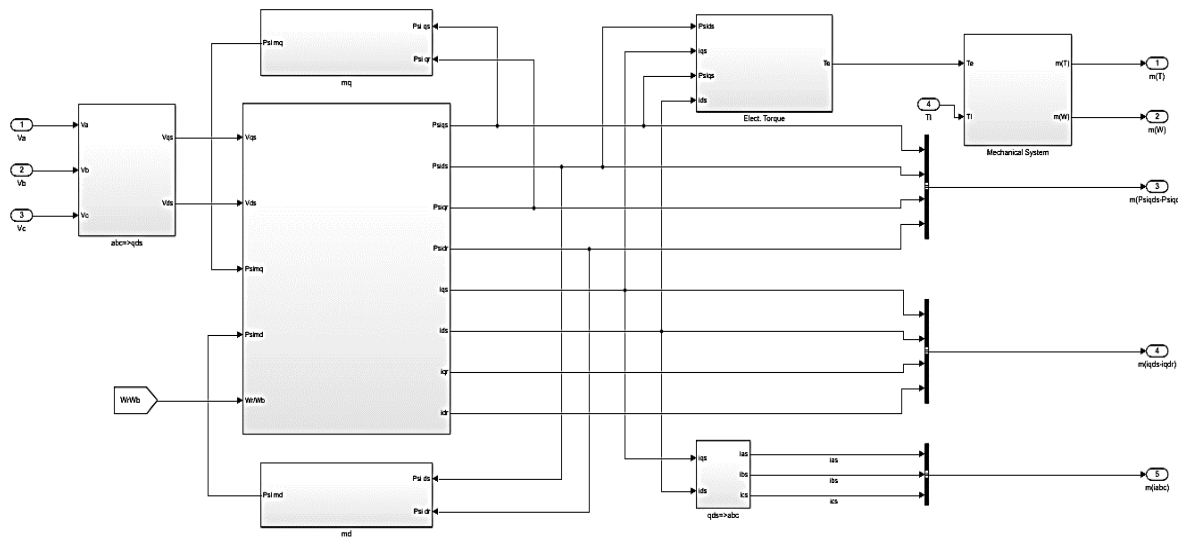

Figure 3. Model of a three-phase induction motor in the stationary reference frame

2.2. Variable speed drive
A space vector PWM drive is developed, which represents a closed-loop (V/f) control drive for an induction motor. The speed of induction motors n is directly proportional to the frequency of the supply f as (22):

$$n = \frac{120f}{no.of\ poles} \tag{22}$$

So, controlling the speed of an induction motor can be done by controlling the supply frequency, but in order to keep the torque of the induction motor constant, the ratio of volts per frequency (V/f) must be kept constant [17]. Conventional proportional-integral (PI) controller can be used to control the speed of induction

motors. The actual speed of the motor n is subtracted from the reference speed n^* to get the error $e(t)$. Then, the reference machine slip n_{sl}^* is generated by the PI controller, which is added to the actual motor speed n. After that, the reference frequency f^* and reference voltage v^* are calculated, and used as an input to the space vector PWM (SVPWM) modulator. Typical induction motor speed control with slip regulation using a PI controller is represented in Figure 4. The proportional-integral (PI) controller has to be tuned to obtain the proportional gain Kp and integral gain Ki parameters. The tuning process could be done by trial-and-error method. But this method requires experience and may not lead to obtaining the optimal values of the gain parameters. Therefore, affects the performance of the speed controller [18], [19]. Also, Cohen-Coon Method and Ziegler-Nichols method [20] can be used to tune the PI controller. A rule-based fuzzy logic speed controller is implemented in the model to replace the conventional PI controller.
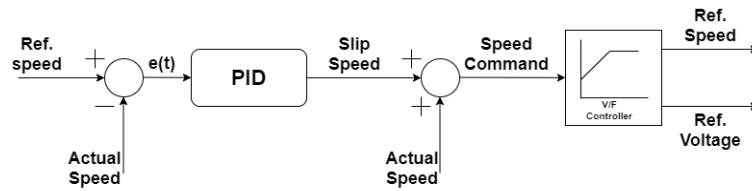

Figure 4. Typical induction motor speed control using a PI controller with slip regulation

2.2.1. Space vector pulse width modulation

Space vector PWM (SVPWM) is one of the PWM switching techniques, which is used in voltage source inverters (VSI). SVPWM represents the inverter output (i.e., three-phase voltages) as a single rotating vector. So, it deals with the three-phase voltages V_a, V_b, and V_c as a single quantity in contrast to the sinusoidal PWM (SPWM) which deals with each phase voltage separately. The Space vector V_{ref} is defined as in (23) [21].

$$\bar{V}_{ref} = \frac{2}{3}(\bar{V}_a + e^{j2\frac{\pi}{3}}\bar{V}_b + e^{j4\frac{\pi}{3}}\bar{V}_c) \tag{23}$$

A two-level voltage source inverter (VSI) is used in the model consisting of six insulated gate bipolar transistors (IGBT) [S1, S2, . . ., S6]. The VSI has three legs, each leg has two IGBT switches as in Figure 5. Each switch has only two states [on and off] and in each leg when the upper switch is on, the lower switch must be off and vice versa. So, the possible number of states of the inverter switches are $2^3 = 8$, as shown in Table 1. For simplification, the reference space vector can be represented in terms of α and β by applying the Clarke transformation as in (24). Figure 6 shows V_{ref} in the first sector.

$$\begin{bmatrix} \bar{V}_\alpha \\ \bar{V}_\beta \end{bmatrix} = \frac{2}{3} \begin{bmatrix} 1 & -\frac{1}{2} & -\frac{1}{2} \\ 0 & \frac{\sqrt{3}}{2} & -\frac{\sqrt{3}}{2} \end{bmatrix} \begin{bmatrix} V_a \\ V_b \\ V_c \end{bmatrix} \tag{24}$$

So V_{ref} can be represented in terms of V_α and V_β as (25):

$$\bar{V}_{ref} = \bar{V}_\alpha + j\bar{V}_\beta = \frac{2}{3}(\bar{V}_a + e^{j2\frac{\pi}{3}}\bar{V}_b + e^{j4\frac{\pi}{3}}\bar{V}_c) \tag{25}$$

Table 1. Possible states of switches in a two-level three-phase VSI

Switching state	S1	S2	S3	Space vector phase to neutral voltage
000	Off	Off	Off	0
001	Off	Off	On	$(2/3)V_{dc}e^{j(4\pi/3)}$
010	Off	On	Off	Off
011	Off	On	On	On
100	On	Off	Off	Off
101	On	Off	On	On
110	On	On	Off	Off
111	On	On	On	On

The space vector PWM (SVPWM) realization algorithm is as (26):

- Step 1: Determine sector number n_{sector} in which the reference space vector is located in

$$n_{sector} = \frac{\alpha(rad)}{2\pi} \qquad (26)$$

- Step 2: Determine reference vector $\bar{V}_{ref}$ value and angle

$$\bar{V}_{ref} = \sqrt{V_\alpha^2 + V_\beta^2} \qquad (27)$$

$$\alpha = \tan^{-1}(\frac{V_\beta}{V_\alpha}) \qquad (28)$$

- Step 3: Applying the 'equal volt-second principle' [22], [23]

$$\bar{V}_{ref}T_s = V_1T_1 + V_2T_2 + V_0T_0 \qquad (29)$$

Where, $\bar{V}_{ref} = |\bar{V}_{ref}|e^{j\alpha}, \bar{V}_1 = \frac{2}{3}V_{dc}e^{j(n-1)\frac{\pi}{3}}, \bar{V}_2 = \frac{2}{3}V_{dc}e^{jn\frac{\pi}{3}}, V_0 = 0$

- Step 4: Calculate T_1, T_2 and T_0

$$T_1 = T_s \frac{\sqrt{3}\bar{V}_{ref}\sin(n_{sector}\frac{\pi}{3}-\alpha)}{V_{dc}} \qquad (30)$$

$$T_2 = T_s \frac{\sqrt{3}\bar{V}_{ref}\sin(\alpha-(n_{sector}-1)\frac{\pi}{3})}{V_{dc}} \qquad (31)$$

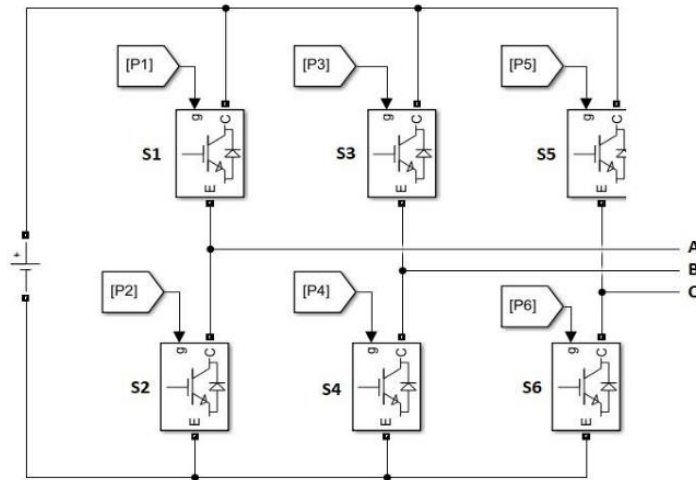$$T_0 = T_s - (T_1 + T_2) \qquad (32)$$
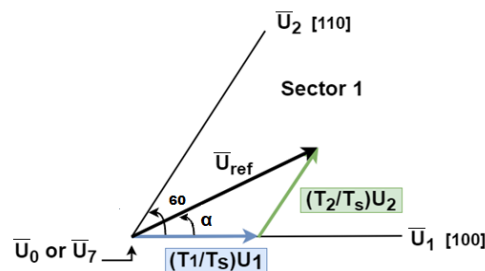

Figure 5. Two-level voltage source inverter

Figure 6. Reference space vector in sector 1

2.2.2. Fuzzy logic controller

Speed control of an ESP motor in this paper is achieved by using a fuzzy logic controller (FLC), instead of the conventional proportional-integral (PI) controller. Fuzzy logic is an approach introduced by Lotfi Zadeh in 1965 [24], to simulate the human-like way of thinking. Unlike Boolean logic in which the value of any object could be either 1 [True] or 0 [False], the value of an object in fuzzy logic could be any value from 0 to 1, which can be described as linguistic variables [25]. For example, to describe temperature, the linguistic variable can be represented as [very cold–cold–mild–hot–very hot]. Fuzzy logic controller basic structure [26], [27] is shown in Figure 7 and it is consisting of:

− Fuzzification process: In this process, the numerical or crisp input variables are converted to linguistic variables to be compatible with the rule base for further processing.
− Knowledge base and inference engine: The knowledge base consists of a rule base and database. The rule base is a combination of linguistic instructions in the form of" IF...THEN..." rules, which determine the value of the output with respect to the input values. Consider an FLC which controls the speed of an induction motor, the controller has two inputs error $e(t)$ and the change of error $ce(t)$ and one output $u(t)$ which is the change in the output, one example of the linguistic rules is" IF error (E) is negative small (NS) AND change in error (CE) is positive small (PS) THEN change in output (DU) is zero (Z)". The database contains the membership functions of the input and output variables, while the inference engine determines the output after applying the rules on the fuzzier inputs.
− Defuzzification process: The fuzzifier carries out transforming the output signal from the fuzzy variables to the crisp variables, so it is the opposite of the fuzzification process.
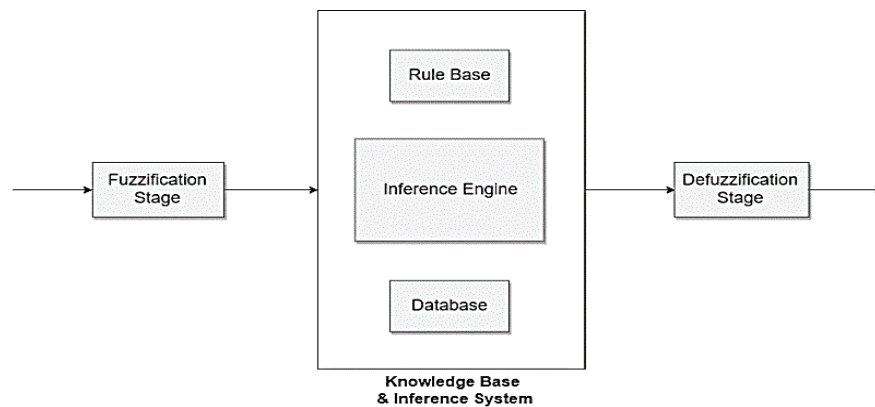

Figure 7. The basic structure of fuzzy logic controller

2.2.3. Fuzzy logic speed controller implementation

The rule-based fuzzy logic (FLC) speed controller used in this paper is shown in Figure 8. It has two input variables, speed error $e(t)$ and change in speed error $ce(t)$, and one output variable slip speed $u(t)$. The feedback signal of the actual motor speed is subtracted from the reference speed signal, to get the speed error $e(t)$. After that, the error $e(t)$ is differentiated to get the rate of change of the speed error $ce(t)$. The Output of the FLC is then added to the actual motor speed to get the speed command which is further processed through the V/f controller to obtain the reference voltage V^* and the reference frequency f^* commands.
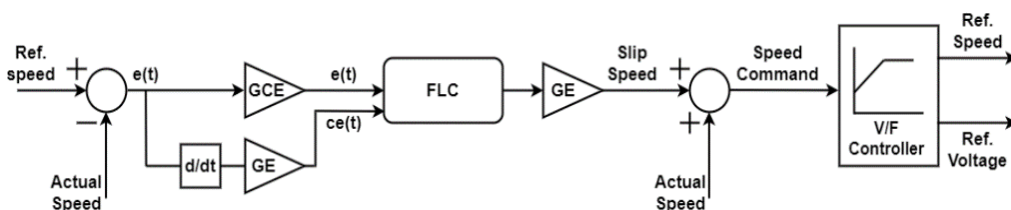

Figure 8. Fuzzy logic-based speed controller

The input and output linguistic variables are [NB=negative big, NM=negative medium, NS=negative small, Z=zero, PS=positive small, PM=positive medium, PB=positive big], The shapes of the membership functions used in the paper are arbitrarily chosen, Gaussian-shaped membership functions (MF) are considered for the input variables as shown in Figure 9(a), triangle-shaped membership functions for the output variables as shown in Figure 9(b) and the linguistic rules are presented in Table 2. The surface view of the FLC rules is shown in Figure 9(c).

Table 2. Linguistic rules

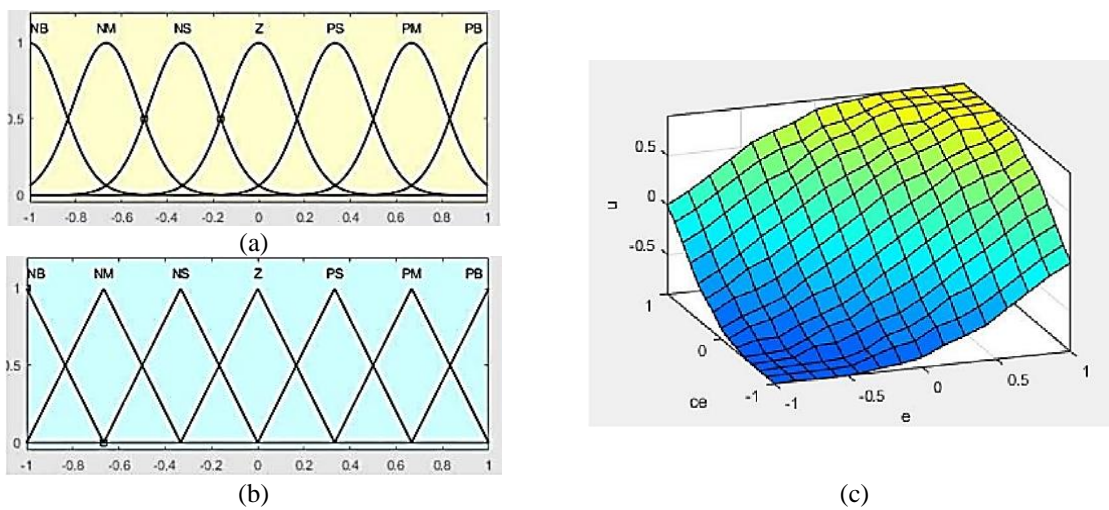| Error Change in error	NB	NM	NS	Z	PS	PM	PB
NB	NB	NB	NB	NM	NS	Z	PS
NM	NB	NB	NM	NS	Z	PS	PM
NS	NB	NM	NS	Z	PS	PM	PB
Z	NM	NS	Z	PS	PM	PB	PB
PS	NM	NS	Z	PS	PM	PB	PB
PM	NS	Z	PS	PM	PB	PB	PB
PB	Z	PS	PM	PB	PB	PB	PB

Figure 9. Membership functions (MF): (a) MFs of the input variables, (b) MFs of the output variables, and (c) the surface view of the FLC rules

2.3. ESP oil well model

In order to create a dynamic model of an electrical submersible pump (ESP) oil well, it can be represented as shown in the simplified schematic of the ESP oil well in Figure 10. This model was originally developed by Statoil [11] and a similar approach was developed by a parallel work [28] which, is used in this paper. The reservoir pressure is P_r and the flow rate which the reservoir can deliver to the well is q_r. Reservoir fluids have viscosity μ and average density ρ_{avg}. The Volume below ESP is considered as a single control volume V_1 with an average flow rate $\bar{q}$, the pressure in the bottom of control volume V_1 is the bottom-hole pressure P_{bh}, while ESP intake pressure P_i is the pressure at the top of control volume V_1. The Volume above ESP is considered also as a single control volume V_2 with an average flow rate $\bar{q}$. The pressure at the top of control volume V_2 is the well-head pressure P_{wh}, while the pressure at the bottom of control volume V_2 is the ESP discharge pressure, and is denoted as P_d.

ESP is located between the two control volumes and its function is to boost the pressure by ΔP_{esp} as (33):

$$\Delta P_{esp} = P_d - P_i = \rho_{avg} g H_{esp} \tag{33}$$

Brake horsepower BHP is the power required by the pump. For one pump stage running at base speed f_0, the head $H_{esp-1stg}$ and brake horsepower $BHP_{esp-1stg}$ can be calculated as in (34) and (35):

$$H_{esp-1stg} = h_0 + h_1\bar{q} + h_2\bar{q}^2 + h_3\bar{q}^3 + h_4\bar{q}^4 + h_5\bar{q}^5 \tag{34}$$

$$BHP_{esp-1stg} = p_0 + p_1\bar{q} + p_2\bar{q}^2 + p_3\bar{q}^3 + p_4\bar{q}^4 + p_5\bar{q}^5 \tag{35}$$

Where, $(h_0, h_1, ..., h_5)$ and $(p_0, p_1, ..., p_5)$ are the polynomial head and BHP coefficients, respectively, and are given by the pump manufacturer or can be estimated from the pump performance curves using linear regression methods. In order to get the total head developed and BHP required by the ESP pump running at any speed f, equations (34) and (35) are multiplied by the number of pump stages n_{stg} and affinity laws are applied [2] as in (36) and (37):

$$H_{esp} = n_{stg}(\frac{f}{f_0})^2 H_{esp-1stg} \qquad (36)$$

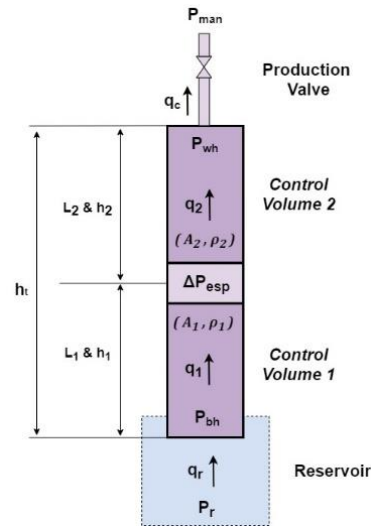$$BHP_{esp} = n_{stg}(\frac{f}{f_0})^3 BHP_{esp-1stg} \qquad (37)$$

Figure 10. Two-volume ESP oil well model

The two-volume ESP oil well model can be represented by the following differential [11], [28].

$$\frac{d\bar{q}}{dt} = \frac{1}{M}[P_{bh} - P_{wh} + \Delta P_{esp} - \frac{\Delta P_{f1}}{A_1} - \frac{\Delta P_{f2}}{A_2} - \rho_{avg}gh_1 - \rho_{avg}gh_2] \qquad (38)$$

$$\frac{dP_{bh}}{dt} = \frac{\beta_1}{A_1 L_1}(q_r - \bar{q}) \qquad (39)$$

$$\frac{dP_{wh}}{dt} = \frac{\beta_2}{A_2 L_2}(\bar{q} - q_c) \qquad (40)$$

Where, M, β_1, and β_2 are the fluid inertia, bulk modulus of fluids below ESP, and bulk modulus of fluids above ESP, respectively. h_1, h_2, A_1, and A_2 are the height of control volume V_1, height of control volume V_2, Area of control volume V_1, and area of control volume V_2, respectively. q_c is the flow rate through the production valve (choke). ΔP_{f1} and ΔP_{f2} are the pressure loss due to friction below and above ESP, respectively. Pressure loss due to friction ΔP_f which occurs in a cylindrical pipe of a uniform diameter D, can be calculated by the Darcy-Weisbach [29] as (41):

$$\Delta P_f = f_D \frac{\rho_{avg}Lv^2}{2D_h} \qquad (41)$$

Where, L and D_h are the length and hydraulic diameter of the pipe, respectively, v is the fluid velocity and f_D is the Darcy friction factor. The inflow from the reservoir into the well depends on P_r and P_{bh}, the simplest way to describe the inflow performance of a well according to [2] is to use the Productivity Index (PI) concept, so the well inflow performance can be represented as (42):

$$q_r = PI(P_r - P_{bh}) \qquad (42)$$

The production valve (choke) can be modeled according to [30] by the following equation, which describes the flow rate through a partially open valve as (43):

$$q_c = kG_c(z_c) \sqrt{P_{wh} - P_{man}} \tag{43}$$

Where, k, G_c, and z_c are the valve constant, valve characteristics, and valve opening, respectively.

3. MODEL AND SIMULATION OF THE COMPLETE SYSTEM

The complete model of the system was done by using MATLAB/SIMULINK® software as shown in Figure 11. The electrical submersible pump mathematical model consists of an ESP motor, ESP pump and dynamic oil well. The ESP motor was modeled as a three-phase induction motor using equations from (5) to (21), and its simulation parameters are shown in Table 3. While, a REDA® 538 SER S8000N ESP pump was modeled by in (36) and (37). Polynomial head and BHP coefficients were estimated from the pump performance curve by using linear regression. The oil well dynamic model was modeled by in (33) and from (38) to (43). ESP pump and oil well model simulation parameters are shown in Table 3.
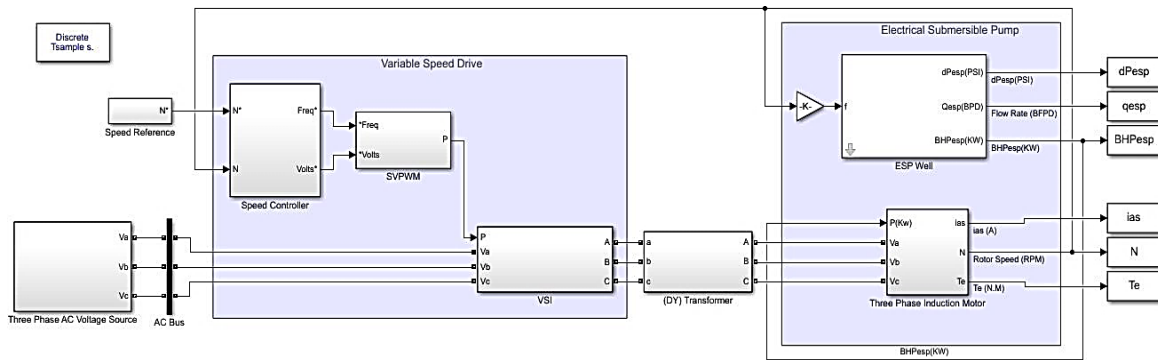

Figure 11. Complete SIMULINK® model of an ESP oil well

Table 3. Complete model simulation parameters

	Parameter	Value	Unit
ESP motor	Power	469	HP
	Voltage	3228	Volts
	Rated speed	2900	RPM
	Number of poles	2	
ESP pump	No. of stages n_{stg}	117	Stage
	h_0	1.32e+01	-
	h_1	6.03e+01	-
	h_2	-9.84e+04	-
	h_3	1.54e+07	-
	h_4	-1.05e+09	-
	h_5	2.09e+10	-
	p_0	7.89e-01	-
	p_1	4.43e+01	-
	p_2	6.85e+03	-
	p_3	-5.22e+05	-
	p_4	6.32e+06	-
	p_5	1.47e-01	-
Oil well	Reservoir pressure (p_r)	3200	PSI
	Productivity index (PI)	7	BPD/PSI
	Fluid specific gravity (SG)	0.87	-
	Fluid viscosity (μ)	1.48	Centipoise
PID controller	Proportional gain (K_p)	0.417	-
	Integral gain (K_i)	4.67	-
FLC controller	GE	0.1	-
	GCE	1e-2	-
	GU	60	-

The model of the variable speed drive was developed, which consists of a rule-based fuzzy logic speed controller, space vector pulse width modulator (SVPWM), and voltage source inverter (VSI). The maximum output voltage of the VSI is 400V, thus, a step-up three-phase transformer was used. A step generator was used to generate the reference speed signal for the speed controller. The acceleration and deceleration rates were set to 7.5 and -7.5 rpm/second, respectively. PID controller proportional K_p and integral K_i gains were obtained using the Ziegler Nichols tuning method. FLC controller gains GE, GCE and GU were arbitrarily chosen. PID and FLC gains are shown in Table 3.

4. RESULTS AND DISCUSSION

In order to evaluate the proposed rule-based fuzzy logic speed controller for the ESP system, the simulation results for both PID and FLC speed controllers were obtained. The proposed simulation scenario is as follows: At [t = 0 seconds], the ESP motor was running normally at 50Hz, then at [t = 10 seconds], the reference speed signal was changed from 50Hz to 56Hz, and the acceleration rate was set to 7.5 rpm/second. First, a simulation was run for the PID speed controller. When the reference speed signal was increased, the ESP motor starts to accelerate till reaching the new target speed value. The rise and settling times are 19.2549 and 23.6226 seconds, respectively. Then, a simulation was run for the FLC speed controller. Similarly, when the reference speed signal was increased, the ESP motor starts to accelerate till reaching the new target speed value. The rise and settling times are 19.1999 and 23.5197 seconds, respectively. Figure 12 shows the ESP speed (N) in rpm versus the reference speed signal. The electromagnetic torque T_e of the ESP motor increased proportionally to the square of the speed change as shown in Figure 13. Also, it is shown from the figure that when the PID speed controller was used, the electromagnetic torque contains many ripples. However, the electromagnetic torque in the case of using the FLC speed controller was very smooth. ESP pump flow rate q increased proportionally to the change of the speed as shown in Figure 14, while brake horsepower (BHP) increased proportionally to the cube of the speed change as shown in Figure 15. Finally, the discharge pressure (P_d) of the ESP pump increased proportionally to the square of the speed change as shown in Figure 16. Table 4 shows a comparison between the results of PID and FLC speed controllers obtained from the simulation. Results show a significant decrease in overshoot and error values when the FLC speed controller was utilized in the system.

Table 4. Comparison of PID and FLC speed controller results

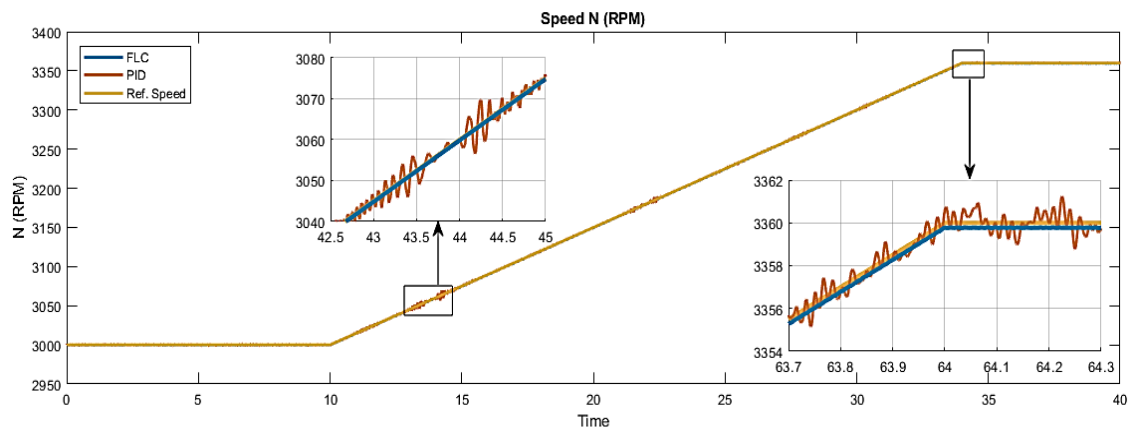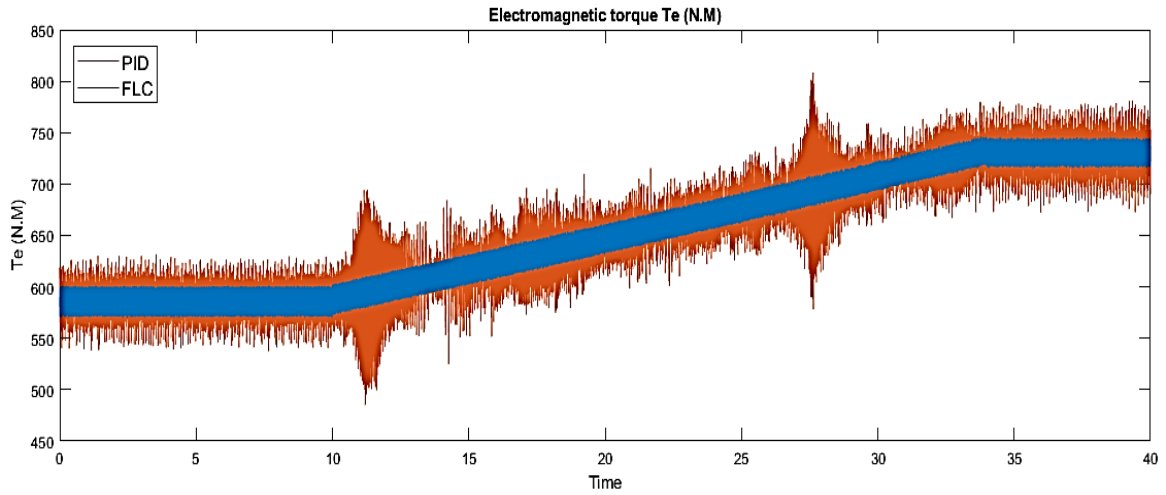|	PID	FLC
Settling time (s)	19.2549	19.1999
Rising time (s)	23.6226	23.5197
Overshoot	0.0256	0.00088
Integral Absolute Error (IAE)	0.4065	0.1487
Integral Square Error (ISE)	0.007428	0.0004987
Integral Time Absolute Error (ITAE)	20.4	8.028
Integral Time Square Error (ITSE)	0.3583	0.02765

Figure 12. ESP motor speed N (RPM)

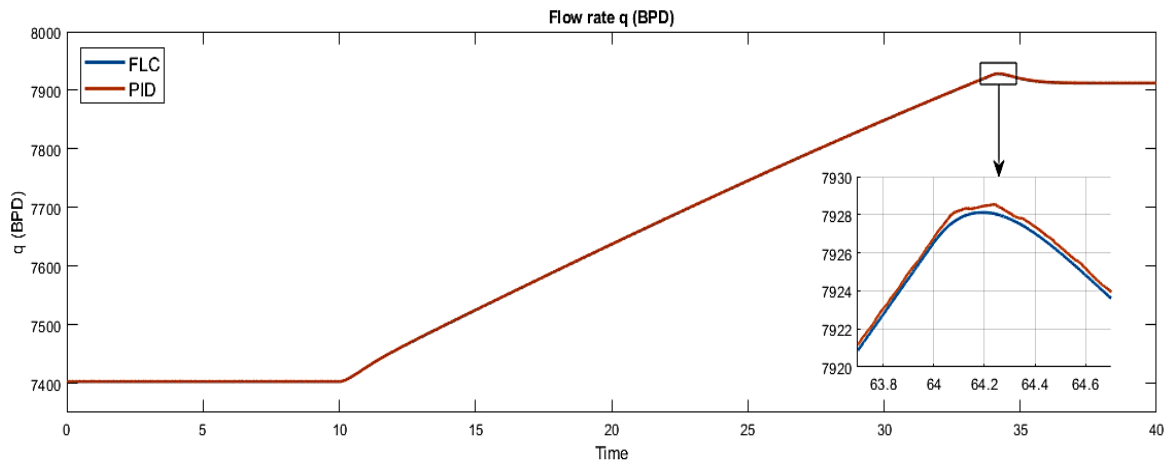Figure 13. Electromagnetic torque Te (N.M) 30

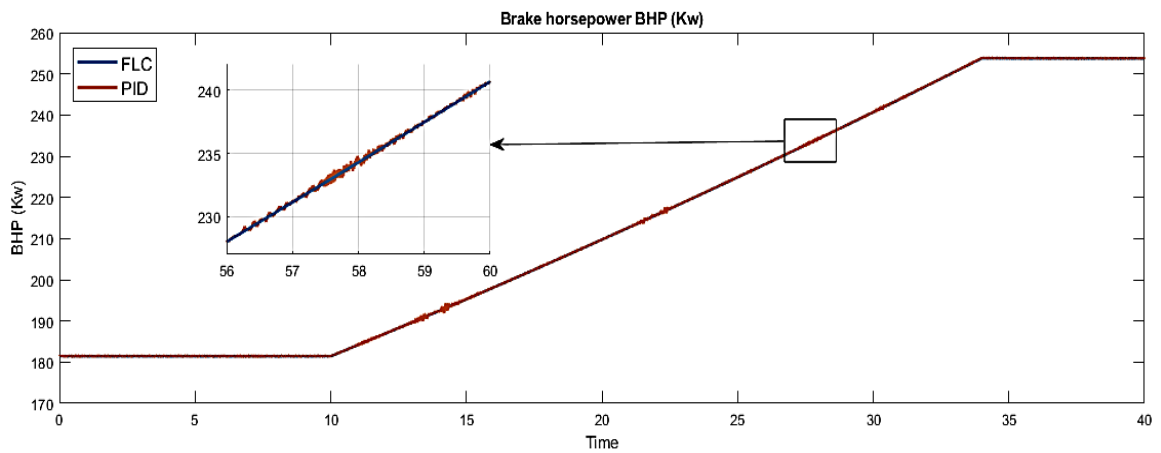Figure 14. Flow rate q (BPD)

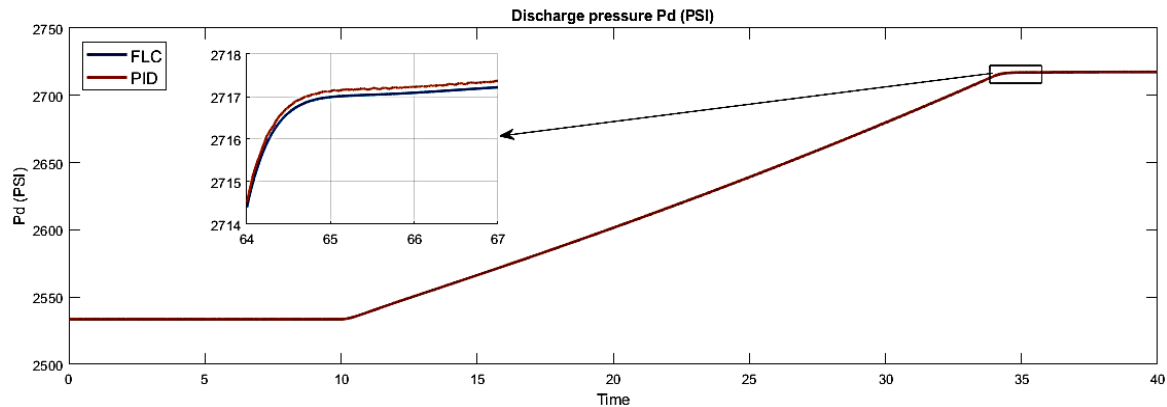
Figure 15. Brake horsepower BHP (Kw)

Figure 16. Discharge pressure Pd (PSI)

5. CONCLUSION

A space vector pulse width modulation (SVPWM) has been used as a PWM switching algorithm. Also, a rule-based fuzzy logic controller has been developed to control the speed of an ESP. In this study, a simulative validation of the complete model has been done. The combination of SVPWM and FLC speed controller has achieved a superior and more effective method of controlling the speed of an ESP when compared to the conventional PID speed controllers. As well, the dynamic model of a case study has been developed and the effects of changing the speed of an ESP on both the pump performance as well as, the motor parameters are analyzed. The developed dynamic model can be employed in many applications such as control and optimization of operations, power consumption, and wells production. In the future, the proposed model will be implemented to control the speed of an ESP oil well in the field, for further verification of the obtained results.

REFERENCES

[1]   R. B. Minogue and A. L. Eiss, "Nuclear regulatory commission regulations and licensing," *Nuclear Power Safety*, pp. 57-86, 1976, doi: 10.1016/B978-0-08-021744-4.50007-5.
[2]   G. Takacs, "Electrical submersible pumps manual: Design, operations, and maintenance," *Gulf Professional Publishing - Elsevier*, 2nd Edition, 2017.
[3]   A. H. VanderMeulen, T. J. Natali, T. J. Dionise, G. Paradiso and K. Ameele, "Exploring new and conventional starting methods of large medium-voltage induction motors on limited kVA sources," *IEEE Transactions on Industry Applications*, vol. 55, no. 5, pp. 4474-4482, 2019, doi: 10.1109/TIA.2019.2922339.
[4]   S. F. Rabbi, J. T. Kahnamouei, X. Liang and J. Yang, "Shaft failure analysis in soft-starter fed electrical submersible pump systems," *IEEE Open Journal of Industry Applications*, vol. 1, pp. 1-10, 2020, doi: 10.1109/OJIA.2019.2956987.
[5]   S. Pham, and D. Tran, "Production optimization of a network of multiple wells with each well using a combination of electrical submersible pump and gas lift," *Journal of Petroleum Exploration and Production Technology*, vol. 12, pp. 631-659, 2022, doi: 10.1007/s13202-021-01313-z.
[6]   H. Kirby, R. Paes and J. Flores, "Speed control of electric submersible pumps - the "current" approach," Fourtieth IAS Annual Meeting," *Conference Record of the 2005 Industry Applications Conference*, 2005, vol. 3, pp. 1908-1918, doi: 10.1109/IAS.2005.1518708.
[7]   A. Sperlich, D. Pfeiffer, J. Burgschweiger, E. Campbell, M. Beck, R. Gnirss, and M. Ernst, "Energy efficient operation of variable speed submersible pumps: simulation of a ground water well field," *Water*, vol. 10, no. 9, pp. 1-12, 2018, doi: 10.3390/w10091255.
[8]   D. Grassian, and D. Olsen, "Detailed energy accounting of electrical submersible pumping systems," *Energies*, vol. 13, no. 2, pp. 1-24, 2020, doi: 10.3390/en13020302.
[9]   T. Poompavai, and M. Kowsalya, "Control and energy management strategies applied for solar photovoltaic and wind energy fed water pumping system: A review," *Renewable and Sustainable Energy Reviews*, vol. 107, pp. 108-122, 2019, doi: 10.1016/j.rser.2019.02.023.
[10]   J. Kullick and C. Hackl, "Dynamic modeling and simulation of deep geothermal electric submersible pumping systems," *Energies*, vol. 10, no. 10, pp. 1-37, 2017, doi: 10.3390/en10101659.
[11]   A. Pavlov, D. Krishnamoorthy, K. Fjalestad, E. Aske and M. Fredriksen, "Modelling and model predictive control of oil wells with Electric Submersible Pumps," *IEEE Conference on Control Applications (CCA)*, 2014, pp. 586-592, doi: 10.1109/CCA.2014.6981403.
[12]   S. F. Rabbi, M. M. Sarker, D. G. Rideout, S. D. Butt, and M. A. Rahman, "Analysis of a hysteresis ipm motor drive for electric submersible pumps in harsh atlantic offshore environments," *Proceedings of the ASME 2015 34th International Conference on Ocean, Offshore and Arctic Engineering OMAE*, 2015, doi: 10.1115/omae2015-41955.
[13]   G. Takacs, "Three inventions shaping the future of ESP technology," *Journal of Petroleum Science and Engineering*, vol. 182, 2019, doi: 10.1016/j.petrol.2019.106330.
[14]   K. S. Gaeid, H. W. Ping and H. A. F. Mohamed, "Simulink representation of induction motor reference frames," *Inernational Conference for Technical Postgraduates (TECHPOS)*, 2009, pp. 1-4, doi: 10.1109/TECHPOS.2009.5412114.
[15]   A. Hamed and A. Hazzab, "Modeling and real-time simulation of induction motor using RT-LAB," *International Journal of Power Electronics and Drive Systems*, vol. 9, no. 4, pp. 1476-1485, 2018, doi: 10.11591/ijpeds.v9.i4.pp1476-1485.

[16] P. C. Krause, "Analysis of electric machinery and drive systems," *John Wiley & Son*, Third edition, 2013.
[17] S. N. Mahsahirun, N. R. Nik Idris, Z. B. Yusof, and T. Sutikno, "Fundamental elements of constant volt/hertz induction motor drives based on dSPACE DS1104 controller," *International Journal of Power Electronics and Drive System*, vol. 11, no. 4, pp. 1670-1685, 2020, doi: 10.11591/ijpeds.v11.i4.pp1670-1685.
[18] H. I. Jaafar, S. Yuslinda, N. Selamat, M. S. M. Aras, and M. Rashid, "Development of pid controller for controlling desired level of coupled tank system," *International Journal of Innovative Technology and Exploring Engineering*, vol. 3, no. 9, pp. 32-36, 2014.
[19] D. Yadav and A. Verma, "Comperative performance analysis of PMSM drive using MPSO and ACO Techniques," *International Journal of Power Electronics and Drive Systems*, vol. 9, no. 4, pp. 1510-1522, 2018, doi: 10.11591/ijpeds.v9.i4.pp1510-1522.
[20] J. G. Ziegler and N. B. Nichols, "Optimum settings for automatic controllers," *Journal of Dynamic Systems*, *Measurement, and Control*, vol. 115, pp. 220–222, 1993, doi: 10.1115/1.2899060.
[21] A. Iqbal, S. Moin, M. Khan, and H. Abu-Rub, "Generalised simulation and experimental implementation of space vector pwm techniques of a three-phase voltage source inverter," *International Journal of Engineering, Science and Technology*, vol. 2, no. 1, pp. 1-12, 2010.
[22] H. Abu-Rub, A. Iqbal, and J. Guzinski, "High performance control of ac drives with MATLAB/simulink models," *John Wiley & Sons*, 2021.
[23] S. Ali, V. Kumar Reddy and M. Kalavathi, "Coupled random PWM technique for dual inverter fed induction motor drive," *International Journal of Power Electronics and Drive Systems*, vol. 10, no. 1, pp. 58-65, 2019, doi: 10.11591/ijpeds.v10.i1.pp58-65.
[24] L. A. Zadeh, "Fuzzy sets," *Information and Control*, vol. 8, no. 3, pp. 338-353, 1965.
[25] B. K. Bose, "Modern power electronics and AC drives," Prentice Hall: Upper Saddle River, NJ, 2002.
[26] F. Gomide, A. Rocha, and P. Albertos, "Neurofuzzy controllers," *IFAC Proceedings*, vol. 25, no. 5, pp. 13-26, 1992, doi: 10.1016/s1474-6670(17)49573-5.
[27] N. Farah, M. Talib, Z. Ibrahim, J. Lazi, M. Azri, "Self-tuning fuzzy logic controller based on takagi- sugeno applied to induction motor drives," *International Journal of Power Electronics and Drive Systems*, vol. 9, no. 4, pp. 1967-1975, 2018, doi: 10.11591/ijpeds.v9.i4.pp1967-1975.
[28] R. Sharma and B. Glemmestad, "Optimal control strategies with nonlinear optimization for an electric submersible pump lifted oil field," *Modeling, Identification and Control (MIC)*, vol. 34, no. 2, pp. 55-67, 2013, doi: 10.4173/mic.2013.2.2.
[29] K. E. Brown, *The technology of artificial lift methods*, Tulsa: PennWell Books, vol. 1, no. 2, 1977.
[30] F. White and H. Xue, *Fluid mechanics*, McGraw-Hill Education, 9th edition., 2021.

BIOGRAPHIES OF AUTHORS

Saleh M. El-koliel 🆔 🇬 SC ⬡ is an electrical field engineer with more than 10 years of experience in oil and gas industry. He is currently working at Qarun petroleum company, Egypt. He received his B.Sc. in Electrical Engineering from Mansoura university Egypt, in 2012. He is currently pursuing his M.Sc. from Al-Azhar university, Egypt. His research interests include the field of power electronics, adjustable speed drives, artificial intelligence and industrial applications. He can be contacted at email: saleh.el.koliel@gmail.com.

Hussein Eleissawi 🆔 🇬 SC ⬡ received the B.Sc. degree in electrical engineering from Zagazig University, Egypt, in 1995, the M.Sc. degree in electrical engineering from Cairo University, Egypt, in 2007, and the Ph.D. degree from Al-Azhar University, Egypt, in 2012. He is a Lecturer with the Reactors Department, Atomic Energy Authority, Egypt, and the Advisor of Electrical engineering systems at ETRR-2 Complex, Egypt. His current research interests include power quality, Light current systems, power electronics, motor drives, renewable energy, nuclear safety, physical protection and management of electrical system. He can be contacted at email: el_eissawi@yahoo.com.

Adel S. Nada 🆔 🇬 SC ⬡ is a full professor at Al-Azhar University, Faculty of Engineering, Electrical Department, Cairo, Egypt. He received his Ph.D. from Al-Azhar University in 2000 (Title: Analysis and Control of a Wind Energy Driven Self-Excited Induction Generator Connected to an Infinite Bus Bar). His areas of interest are Electrical Machines, Power electronics, and Renewable Energy, especially Wind and Solar Energy. He participated in many research papers published in many international journals. He is an entrepreneur and expert at General Organization for Physical Planning in Egypt. He can be contacted at email: adel.saad1@hotmail.com.